Off-resonant preparation of a vibrational coherence for enhanced stimulated Raman scattering

S. Gundry, M. P. Anscombe, A. M. Abdulla, S. D. Hogan, E. Sali, J. W. G. Tisch, and J. P. Marangos
Blackett Laboratory, Prince Consort Road, South Kensington, Imperial College, London SW7 2BZ, United Kingdom
(Received 10 May 2005; published 27 September 2005)

We present a detailed experimental investigation into the off-resonant preparation of a vibrational coherence for multiorder Raman generation. In particular, the importance of the balance between the conflicting requirements for generating a strong coherence and for adiabatic evolution of the system are examined. For the parameters accessible in our experiment, we find that the strongest frequency modulation occurs under conditions for which there is some nonadiabatic behavior, and the coherence is less than the peak value obtainable. We investigate the modulation of a narrowband probe pulse, and an ultrashort probe pulse, in the coherently prepared medium, and demonstrate efficient modulation of both probe pulses resulting in the generation of 360 THz bandwidth fields. This system therefore has an application in the field of subfemtosecond pulse generation.

DOI: 10.1103/PhysRevA.72.033824 PACS number(s): 42.50.Gy, 42.65.Re, 42.65.Dr, 33.80.−b

I. INTRODUCTION

Over recent years, methods involving the preparation of a material coherence have been successfully used in many applications, perhaps most notably in demonstrations of increased efficiency of four-wave mixing, efficient population transfer, and increased transparency of a medium to a resonant laser field (electromagnetically induced transparency and coherent population trapping) [1–7]. The most commonly used technique to prepare a coherence involves the application of two laser fields in resonance with the allowed transitions in a three-level system, the coherence being prepared on the third (single-photon-forbidden) transition in that system. However, in 1994, Harris suggested that a strong coherence can also be induced between two essentially isolated levels in a far-off-resonant scheme [8,9]. Subsequent experimental work, mainly in the field of coherently enhanced Raman generation [10–12], confirmed that off-resonant schemes coupled by intense fields can indeed generate near-maximal levels of material coherence. This scheme is particularly suited to multiorder Raman applications, since a very large range of sideband frequencies are far from resonance with any dipole-allowed transition in the medium, and can therefore propagate without absorption, and with smooth dispersion. Due to the large bandwidths that can be generated, such schemes have recently found application in the field of subfemtosecond pulse generation [13,14].

The laser parameters suitable for off-resonant coherence preparation have previously been investigated theoretically [9,15]. In this paper, we present a detailed experimental study into the preparation process for the application of multiorder Raman generation. We find that the most efficient generation of Raman sidebands, and therefore the strongest frequency (or amplitude) modulation of the input fields, does not occur when the largest magnitude of coherence obtainable is prepared. This is due to the effects of nonadiabatic behavior in the evolution of the system. We also interrogate the coherence using both low-power (0.02 GW cm^{-2}) narrowband, and high-power (10 GW cm^{-2}) ultrashort probe pulses (130 fs), and investigate the maximum achievable efficiency of probe field modulation in both cases. Both systems can potentially generate tunable trains of subfemtosecond pulses. In particular, the modulation of the ultrashort probe field has application to the generation of short trains of high-power subfemtosecond pulses, and even of isolated subfemtosecond pulses [16,17].

In Sec. II, a simple theoretical model for the system of interest is reviewed. Experimental details are then given in Sec. III. In Sec. IV, we present experimental results concerning both the preparation of the coherence, and the introduction of probe fields to the system. Section V then contains a discussion of the results. Conclusions are then presented in Sec. VI.

II. THEORETICAL DISCUSSION

The generation of a strong coherence by the application of two strong off-resonant laser fields has previously been analyzed by a number of authors [9,15,18]. The notation followed here is that of Le Kien *et al.* [15]. The scheme of interest is depicted in Fig. 1; $|a\rangle$ and $|b\rangle$ are vibrational

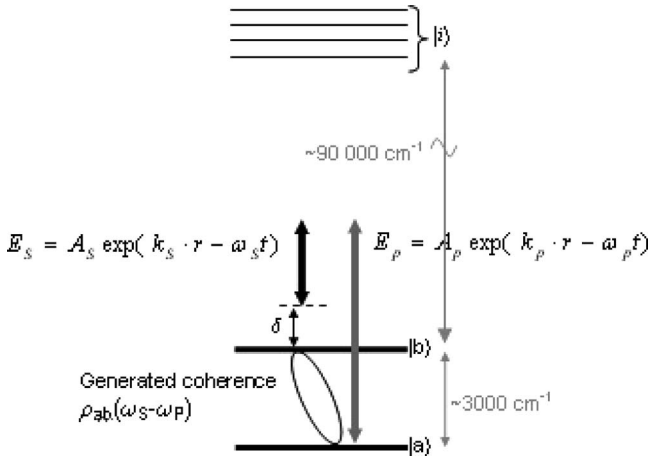

FIG. 1. Scheme for preparation of a large coherence using two strong applied laser fields. Detuning δ shown as negative.

eigenstates of the bare molecular Hamiltonian, while the upper states $|i\rangle$ are the bare electronic eigenstates. We apply two driving fields (termed pump and Stokes) to the system, with a frequency difference that is close to the frequency of the vibrational transition between states $|a\rangle$ and $|b\rangle$: we allow for a small two-photon detuning, defined by $\delta\,[=\omega_{ba}-(\omega_P-\omega_S)]$.

If it is assumed that the population residing in the upper states $|i\rangle$ is negligible, and that the detunings from single-photon resonance are large such that states $|i\rangle$ can be adiabatically eliminated, the time dependence of this system has been shown to be described by the effective two-level Hamiltonian operator [15,18]

$$H_{eff}=-\begin{pmatrix}\Omega_{aa} & \Omega_{ab}\\ \Omega_{ba} & \Omega_{bb}-\delta\end{pmatrix}, \tag{1}$$

where Ω_{aa} and Ω_{bb} are the Stark shifts of levels a and b, given by

$$\Omega_{aa}=\frac{1}{2}\sum_q a_q|E_q|^2, \tag{2a}$$

$$\Omega_{bb}=\frac{1}{2}\sum_q b_q|E_q|^2 \tag{2b}$$

(the summation index q denotes each field present in the system), and the two-photon Rabi frequency Ω_{ab} associated with the two-photon transition is

$$\Omega_{ab}=\Omega_{ba}^*=\frac{1}{2}\sum_q d_q E_q E_{q+1}^*. \tag{3}$$

The constants a_q, b_q, and d_q are the coupling parameters of the specific medium and transition involved, the full expressions for which are given in [15].

The eigenstates of this Hamiltonian, and associated eigenvalues, have been shown to be [15]

$$|+\rangle=\cos\,\theta^{(+)}|a\rangle+\sin\,\theta^{(+)}e^{-i\phi}|b\rangle, \tag{4a}$$

$$|-\rangle=\cos\,\theta^{(-)}|a\rangle-\sin\,\theta^{(-)}e^{-i\phi}|b\rangle, \tag{4b}$$

$$\lambda^{(+)}=\frac{1}{2}(\Omega_{aa}+\Omega_{bb}-\delta)+\frac{1}{2}\sqrt{(\Omega_{aa}-\Omega_{bb}+\delta)^2+4|\Omega_{ab}|^2}, \tag{5a}$$

$$\lambda^{(-)}=\frac{1}{2}(\Omega_{aa}+\Omega_{bb}-\delta)-\frac{1}{2}\sqrt{(\Omega_{aa}-\Omega_{bb}+\delta)^2+4|\Omega_{ab}|^2}, \tag{5b}$$

where (if we express $\Omega_{ab}=|\Omega_{ab}|e^{i\phi}$)

$$\tan\,\theta^{(\pm)}=\frac{2|\Omega_{ab}|}{\Omega_{aa}-\Omega_{bb}+\delta\pm\sqrt{(\Omega_{aa}-\Omega_{bb}+\delta)^2+4|\Omega_{ab}|^2}}. \tag{6}$$

At the beginning of the preparation process, all fields have zero amplitude, and [from Eq. (5)] if $\delta\neq 0$, the eigenstates are nondegenerate, their eigenvalues being given by

$$\lambda^{(+)}=\frac{-1}{2}\delta+\frac{1}{2}|\delta|, \tag{7a}$$

$$\lambda^{(-)}=\frac{-1}{2}\delta-\frac{1}{2}|\delta|. \tag{7b}$$

Depending on the sign of δ, one of these eigenstates is thus coincident with state $|a\rangle$ (which in the interaction picture has zero energy) at the beginning of the process: if $\delta>0$ or $\delta<0$, it is the $|+\rangle$ or $|-\rangle$ state that coincides with state $|a\rangle$, respectively. Therefore, if we assume that at the beginning of the process all population that is not in the upper states $|i\rangle$ resides in state $|a\rangle$, the sign of δ becomes critical in determining which of the two possible eigenstates is populated at the beginning of the process.

The coherence induced on the Raman transition, being defined by $\rho_{ab}=c_a c_b^*$ (where c_i is the probability amplitude of state $|i\rangle$ in the superposition eigenstate) is closely related to the mixing angle defined by $\tan\,\theta$ [15]:

$$\rho_{ab}^{(\pm)}=\cos\,\theta^{(\pm)}\sin\,\theta^{(\pm)}e^{i\phi}=\frac{1}{2}e^{i\phi}\sin 2\theta^{(\pm)} \tag{8}$$

$$=\pm\frac{\Omega_{ab}}{\sqrt{(\Omega_{aa}-\Omega_{bb}+\delta)^2+4|\Omega_{ab}|^2}}. \tag{9}$$

Maximal coherence corresponds to the situation in which the probability amplitudes c_a and c_b are equal, and therefore $\tan(\theta)=1$, and $|\rho_{ab}|=0.5$. It can be seen from Eq. (9) that the inequality

$$\frac{4|\Omega_{ab}|^2}{(\Omega_{aa}-\Omega_{bb}+\delta)^2}\gg 1 \tag{10}$$

must be satisfied if maximal coherence is to be achieved, thus specifying the minimum drive field two-photon Rabi frequency (for a given value of δ) required. The coherence defined in Eqs. (8) and (9) is proportional to the third-order polarization at the Stokes (and anti-Stokes) frequency in the medium. Both the generation of Raman sidebands of the driving fields themselves, and that of any probe field in the system, should therefore be strongest if maximal coherence is attained.

It can be shown that the coherence associated with state $|+\rangle$ oscillates in phase with Ω_{ab}, whereas that associated with the state $|-\rangle$ oscillates out of phase with Ω_{ab} [15]. The π-phase shift in the generated sidebands as the detuning is varied through two-photon resonance has been observed experimentally by Sokolov *et al.* [19]. If the ensemble-averaged coherence is to be large, it is therefore important that only a single eigenstate is excited. Having initially selected a single eigenstate of the Hamiltonian by the choice of δ, it is then imperative to ensure that this state remains to be populated throughout the evolution of the system. For example, if we set $\delta<0$ to select the antiphased state, we do not want the phased state to become populated by transitions from the antiphased state as the field amplitudes evolve. We therefore require that the applied fields do not strongly drive

the transition between the $|+\rangle$ and $|-\rangle$ eigenstates: that is, that the evolution of the system is adiabatic. It has been shown by Le Kien *et al.* [15] that the system will evolve adiabatically provided

$$|\dot{\theta}| \ll |\lambda_+ - \lambda_-|, \tag{11}$$

where the overdot refers to the time derivative. The time derivative of the mixing angle is given by

$$\dot{\theta} = \frac{\delta\Omega_{ab}}{(\lambda_+ - \lambda_-)^2}, \tag{12}$$

and therefore it can be shown [15] that Eq. (11) can be written as

$$|\Omega_{ab}^{(0)}| \ll T\delta^2, \tag{13}$$

where $\Omega_{ab}^{(0)}$ is the peak two-photon Rabi frequency, and T is the full width at half maximum pulse duration, and it has been assumed that

$$|\Omega_{ab}|_{\max} = \frac{|\Omega_{ab}^{(0)}|}{T}. \tag{14}$$

Inspection of Eq. (13) shows that, to ensure adiabatic evolution of the system, it is necessary to either detune very far from two-photon resonance, or apply weak driving fields of low two-photon Rabi frequency. However, both of these requirements conflict directly with those for preparation of a strong coherence [Eq. (10)]. Values of T, Ω_{ab}, and δ must therefore be found that strike the optimum compromise between these two conflicting sets of requirements: in Sec. IV, we present detailed experimental results investigating this balance.

Equation (13) also reveals another important motivation for this work: due to the T dependence, ultrashort ($T < 100$ fs) laser pulses are found to be unsuitable for the generation of a strong coherence through adiabatic evolution. The generation of short trains of pulses by the high order stimulated Raman scattering (HSRS) of ultrashort fields therefore necessitates the coherence to be first prepared by nanosecond pulses. Ultrashort pulses can be used to prepare a coherence in the impulsive and transient regimes [20–22]; however, off-resonant preparation and adiabatic evolution as investigated in this work offer significant advantages. In contrast to impulsive preparation, the scheme we investigate is inherently selective in the Raman transition excited, the maximum frequency of which is not limited by the bandwidth of the driving laser field. The low pulse powers employed in these schemes [17] also result in the avoidance of nonlinear effects, which were observed in recent studies of transient preparation of a coherence [20].

It should be noted that it has been predicted theoretically [9] that if preparation of the medium excites the antiphased state (two-photon excitation *above* resonance), the change of refractive index is more favorable than if the medium is prepared in the phased state, the dispersion at different sideband frequencies being suppressed in the former case, and enhanced in the latter. Le Kien *et al.* have shown explicitly that through propagation, this effect has the result that the coherence generated is larger for small negative δ (above resonant excitation of the antiphased state) than for the small positive δ of the same magnitude (below resonant excitation of the phased state). This is because the reduced dispersion of the antiphased state allows the fields to propagate together over a longer effective interaction length [15]. However, there is some discrepancy in the experimental results on this point; Hakuta and co-workers have found that sideband generation is most efficient when driven above resonance in the antiphased state [12], a result consistent with their theoretical predictions, whereas Harris and co-workers have observed most efficient sideband generation if the medium is prepared in the phased eigenstate with driving fields tuned below resonance [10,11]. It has been suggested that the observation of more efficient sideband generation from the phased state is due to Raman self-focusing [23]. Our results provide further evidence that preparation of the phased state can result in the most efficient modulation of both the driving and probe fields (see Sec. IV).

III. DESCRIPTION OF THE EXPERIMENT

In this work, we prepare a strong coherence on the fundamental vibrational transition in a sample of gaseous D_2 (2993.5 cm^{-1}). D_2 is a suitable choice of gas for this work due to its widely spaced vibrational levels, and has also been used in previous work [10]. The D_2 is contained in a cylindrical cell of length 50 cm, which is immersed in a reservoir of liquid nitrogen to produce a constant D_2 temperature of 77 K along the whole interaction length. Cooling is necessary both to increase the population in the ground rotational state (the Boltzmann factor between the $v=0$, $J=1$ and $v=0$, $J=0$ states in D_2 is 0.49 and 1.125 at temperatures of 77 and 300 K, respectively), and to decrease the Doppler linewidth of the Raman transition (260 MHz at 77 K [10]). In order to avoid ice forming on the cell windows, a vacuum jacket surrounds both the cell and the reservoir. The gas pressure used is typically 150–650 mbar (measured at 77 K).

The pump and Stokes driving fields preparing the coherence are at wavelengths of 807.07 and 1064.19 nm, respectively. These fields are more than 90 000 cm^{-1} from resonance with any allowed single-photon transition in the system. The Stokes field is produced by a Continuum Powerlite 7010 injection seeded neodymium-doped yttrium aluminum garnet (Nd:YAG) laser system producing 10 ns, 80 MHz bandwidth pulses of maximum energy 200 mJ. The tunable pump field is produced by a Continuum HRL-100Z optical parametric oscillator–(OPO-)based laser system consisting of a length-stabilized oscillator, pumped by the second harmonic of the same Nd:YAG laser that generates the Stokes driving field. The oscillator output is then amplified by multiple passes through Nd:YAG-pumped Ti:sapphire crystals. The overall output of this laser system is 4.5 ns, 200 MHz bandwidth pulses of maximum energy 7 mJ [24].

Both driving fields are loosely focused through the cell to provide a peak intensity approaching 1 GW cm^{-2}, while maintaining a relatively long interaction length. The main limitation was found to be that for the focusing to have a long confocal parameter as desired, the beam waist would be

large, meaning that the energy needed to reach the required intensity would be high enough to exceed the damage threshold of the cell windows. Two focusing conditions were therefore identified, both of which were tested in the experiment. The first geometry produces focusing with a long Rayleigh length (24 cm), but slightly lower intensity at the focus (0.55 and 0.36 GW cm^{-2} for the pump and Stokes beams, respectively). This geometry is used for all work involving probe fields. The second geometry results in a slightly shorter Rayleigh length (8.9 cm), but a higher focal intensity (0.9 and 2.4 GW cm^{-2} for the pump and Stokes beams, respectively), and was used as a comparison to the longer-focal-length case in order to investigate the intensity dependence of the coherence preparation process.

The narrowband probe pulse used to interrogate the coherence was derived from the output of a Continuum Mirage 500 laser system; a tunable OPO-based system very similar to the HRL-100Z laser producing the driving field, but utilizing beta barium borate (BBO-)based optical parametric amplifiers to amplify the OPO output, rather than the Ti:sapphire-based system of the HRL-100Z. This system was tuned to produce 800 nm pulses of maximum energy 6 mJ. This output was frequency doubled in a 7-mm-thick BBO crystal to generate the 400 nm probe field of maximum energy roughly 0.5 mJ. All laser systems were triggered externally such that the probe pulse could be injected into the cell at a variable delay with respect to the driving pulses, to an accuracy of ±0.5 ns (limited by temporal jitter in both OPO outputs). The probe beam was focused through the cell with a similar spot size (520 ± 15 μm) and confocal parameter (29.2 ± 3.0 cm) to that of the driving fields. The focal intensity of the probe beam inferred from the measured beam waist is 0.02 GW cm^{-2}; an order of magnitude lower than that of either driving beam due to the reduced pulse energy.

The ultrashort probe beam is derived from a Ti:sapphire-based chirped pulse amplification (CPA) laser system producing 70 fs pulses with a maximum energy of 40 mJ, although lower energies were employed in this experiment. A 2-mm-thick potassium dihydrogen phosphate (KDP) crystal was used to frequency-double the output of this laser, producing 130 fs pulses at 397 nm with a maximum energy of roughly 2 mJ. The pulse duration at 397 nm was limited by the phase-matching bandwidth set by the thickness of the doubling crystal. This beam was down-collimated by a factor of roughly 5 and passed through the cell at a diameter of 2.4 mm and intensities of 10 GW cm^{-2}. It was not possible to subsequently focus this beam to a similar beam waist to the driving fields due to practical limitations on the maximum focal length of the lens used. However, it was found that the relatively large diameter of the ultrashort beam had the important advantage that variation in the pointing direction of the probe field had only a small effect on its spatial overlap with the driving fields. Due to the long path length from the output of the Ti:sapphire compressor to the entrance of the Raman cell (roughly 10 m), the position of the probe beam at the cell entrance was found to drift by as much as 1 mm: however, in a beam size of 2.4 mm, this drift did not significantly affect the overlap of the beams. The lasers generating the driving fields were triggered at a variable delay from a signal derived from the Ti:sapphire CPA system. The accuracy in the delay setting was measured as ±0.3 ns, which was again limited by temporal jitter in the OPO output.

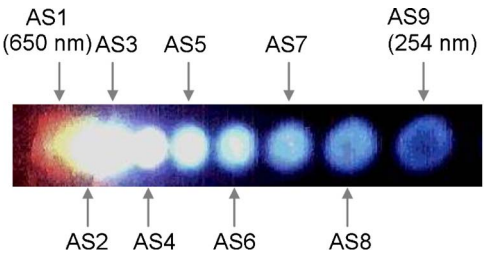

FIG. 2. (Color online) Dispersed cell output for $\delta\approx200$ MHz showing nine anti-Stokes sidebands (AS1–AS9). The infrared driving fields are not visible. Sidebands AS1–3 are partially obscured by camera saturation.

All lasers used in this work operate at a repetition rate of 10 Hz. The light exiting the cell was divided such that the signal could be simultaneously spectrally resolved, and the total output power monitored. The spectrometer used was an Ocean Optics USB2000 fiber-coupled spectrometer, which allows simultaneous detection of all anti-Stokes sidebands generated. A prism was also included in the output path to allow the sideband spectrum to be viewed on a screen.

IV. RESULTS

In this section, we present the results of our investigations into the preparation of a coherence using two far-off-resonant driving fields, and the feasibility of using this coherence to modulate probe fields. Results concerning the preparation of the coherence, and the modulation of the driving fields themselves, are presented in Sec. IV A. Particular emphasis is placed on experimental evidence for the presence and effects of any nonadiabatic behavior in the system, and how this is affected by the value of the detuning δ. Results concerning the modulation of the narrowband probe field are then presented in Sec. IV B. In Sec. IV C, results demonstrating the efficient modulation of the ultrashort probe pulse in the coherently prepared medium are presented.

A. Preparing the coherence: Drive field modulation

When employing the shorter-focal-length geometry of the driving fields, detunings of a few hundred megahertz, pressures of 200–600 mbar, and maximum input driving field intensities, a beam of white light was observed at the cell exit. When dispersed with a prism and viewed on white paper, nine orders of anti-Stokes sidebands were observed (labelled AS1–9), as shown in Fig. 2. At larger magnitude detunings, the output appeared to be strongly dominated by the first anti-Stokes sideband at 650 nm, the cell output taking a strong pink color. When either driving field was propagated through the cell alone, no sidebands were observed.

As shown in Fig. 2, the first six sideband orders were emitted collinearly; a characteristic of Raman generation in a high-coherence regime, in which the refractive-index modification causes self-organized phase matching [25]. These sidebands were observed to have a similar divergence to the

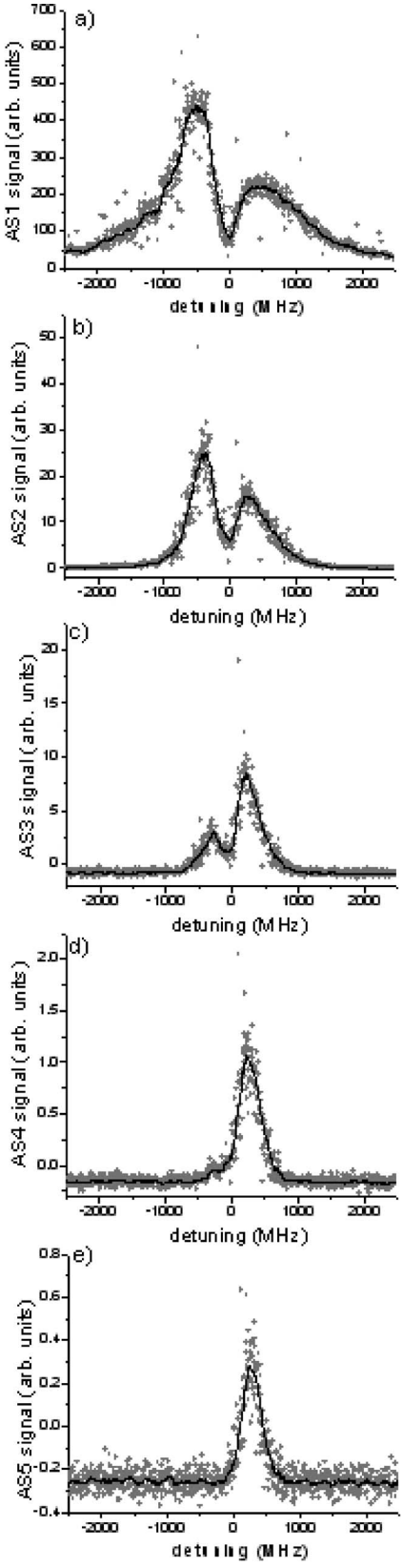

FIG. 3. Dependence of sideband signals on detuning δ_s of driving fields for short-focal-length setup; sideband (a) AS1, (b) AS2, (c) AS3, (d) AS4, and (e) AS5. Black lines show 20-point smoothing of data.

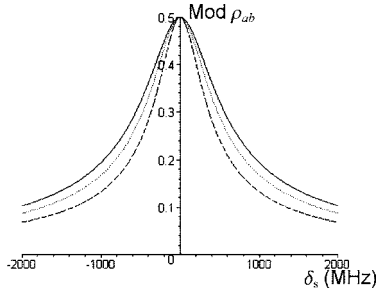

FIG. 4. Calculated variation of coherence magnitude with detuning for input pump field energy of 7 (solid line), 5 (dotted line), and 3 mJ (dashed line). Stokes input energy is constant at 30 mJ.

driving fields. The highest-order sidebands observed (seventh to ninth) were found to be slightly more divergent, and exhibit a more ringlike structure. This is characteristic of the increasing importance of noncollinear phase matching for these sidebands, which are generated after a longer propagation length due to the cascade nature of the process. The collinear nature of the first six anti-Stokes sidebands was preserved for pressures up to approximately 650 mbar. If the pressure was increased beyond this value, a ringlike structure was observed in all anti-Stokes sidebands (Stokes sidebands were not visible by eye). This is due to the increased importance of collisional dephasing of the coherence at higher pressures, the rate of which (450 kHz/torr [10]) becomes equal to the pump laser pulse duration (4.5 ns) at a pressure of 650 mbar. Similar behavior has previously been observed by Sokolov *et al.* [10]. All data presented in this paper were therefore taken using a maximum D_2 pressure of 500 mbar, such that the effects of collisional dephasing could be assumed negligible.

Figure 3 shows how the generated intensity of sidebands AS1–5 (recorded simultaneously) depends on δ_s, the two-photon detuning of the drive fields from the Stark- and pressure-shifted resonance. At the detuning found to generate the highest-order sideband observed (AS5) most efficiently (227 ± 24 MHz), the average efficiency with which energy was transferred from sideband AS1 to sideband AS4 was found to be 0.75 ± 0.04 %.

A simple calculation of the δ dependence of the single-molecule coherence [based on Eq. (9)] for the relevant laser parameters is shown in Fig. 4. Figure 3 shows that sidebands AS1–3 exhibit the basic detuning characteristics calculated in Fig. 4; however, a severe decrease in the sideband signal near to the Stark-shifted resonance ($\delta_s = 0$) is observed. Strong asymmetry as a function of δ_s is observed in sidebands AS4 and AS5. Therefore, although the coherence is maximal when the driving fields are tuned to the Stark-shifted resonance, the generated sideband yield is not greatest at this point.

To further study the effect of δ_s on the output of the system, the total energy transmitted through the cell was recorded simultaneously with the AS1 signal, as shown in Fig. 5 for three different values of the driving field two-photon Rabi frequency. This figure clearly shows that there is a loss in energy transmitted through the cell for all three data sets, which is dependent on the pump field frequency (and there-

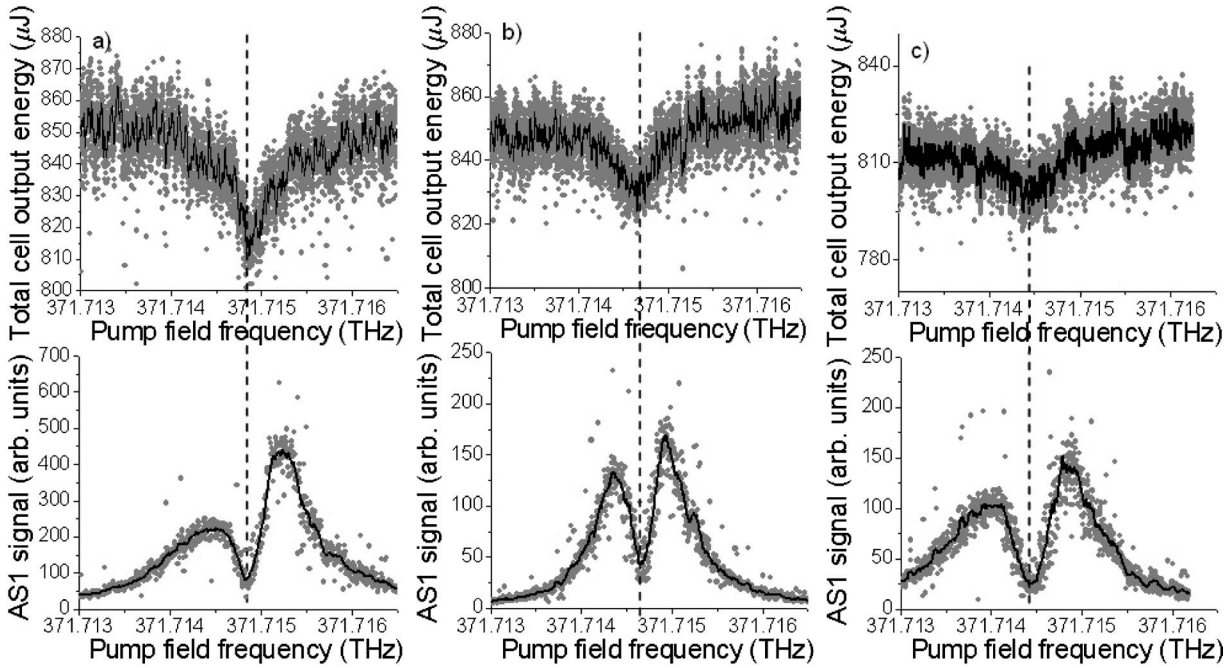

FIG. 5. Short focusing geometry. (a) Total energy transmitted through cell, and generated intensity of first-order anti-Stokes sideband as a function of pump field frequency at input pump field energy 4.52±0.30 mJ (two-photon Rabi frequency=50 MHz). (b) Same as (a), except at input pump field energy 3.11±0.22 mJ (two-photon Rabi frequency=41 MHz). (c) Same as (a), except at input pump field energy 2.13±0.16 mJ (two-photon Rabi frequency=34 MHz). Black line is 20-point smoothing of data.

fore on δ). Table I shows how the fractional energy loss in the cell varied with the applied driving field two-photon Rabi frequency (Ω_{ab}). The energy loss is found to be greater as Ω_{ab} is increased. This behavior is consistent with the formalism describing adiabatic following [Eq. (13)]. The maximum of this energy loss is found to occur at the same pump field frequency as produces the local minimum in the sideband AS1 signal, suggesting that the cause of the decreased signal near two-photon resonance is nonadiabatic behavior. This point is discussed further in Sec. V.

If the longer focusing geometry is employed, there is an observable change in the detuning characteristics of the driving field sidebands (see Fig. 6). The decrease in the signal of sideband AS1 at small detunings is found to be less severe than for the tighter focusing case presented in Fig. 3. This is consistent with the evolution of the system being more adiabatic, as expected for the focusing geometry in which the two-photon Rabi frequency is smaller. However, the maximum conversion efficiency (0.33±0.09 %) is found to be lower by approximately a factor of 2. This implies that although the process is more adiabatic, the coherence is also weakened by the decrease in the two-photon Rabi frequency of the driving fields.

TABLE I. Fractional energy loss in cell for different-driving-field-applied two-photon Rabi frequencies.

Ω_{ab} (MHz)	Fractional energy loss
50	$(2.87\pm0.08)\times10^{-2}$
41	$(1.91\pm0.08)\times10^{-2}$
34	$(1.36\pm0.06)\times10^{-2}$

B. Probing the coherence with a third narrowband input field

As an independent probe of the material coherence induced by the driving fields, we next introduced a transform-limited probe pulse of duration 3.5 ns, and center wavelength 400 nm into the cell, synchronously with the driving fields. We observe significant modulation of the probe field (see Fig. 7): for clarity, the anti-Stokes sidebands of the driving fields are labeled as before (AS1, AS2, etc.), whereas the sidebands of the probe field are labeled PAS1, PAS2, etc. It should be emphasized that the probe field is far from resonance with any allowed transition in the system: the detuning δ_s refers to the two-photon detuning (from the Stark-shifted resonance) with which the driving fields prepare the modulator.

At zero probe pulse delay (temporal coincidence with the peak of the driving fields, to an accuracy of ±0.5 ns), two Stokes and two anti-Stokes sidebands of the probe field were observed for values of δ_s in the range 0–200 MHz, and pressures of 150–250 mbar, as shown in Fig. 7. If propagated through an unprepared sample at the same intensity and pressure, no sidebands of the probe field were observed.

Figure 8 shows the dependence of the generated probe field sideband intensities on δ_s, the detuning of the driving fields from the Stark-shifted resonance. As for the driving fields themselves, the most efficient modulation occurs at a nonzero value of δ_s (δ_s=74.6±30.0 MHz). This result confirms that a third pulse can be modulated by the coherence created by the driving pulses, as has been found previously by Liang *et al.* [12]. At δ_s=74.6±30.0 MHz, the efficiency of generation of sidebands PAS1, PAS2, and PS1 is found to be 0.86±0.09 %, 0.038±0.004 %, and 0.19±0.02 %, respectively. All probe field sidebands are observed to have a

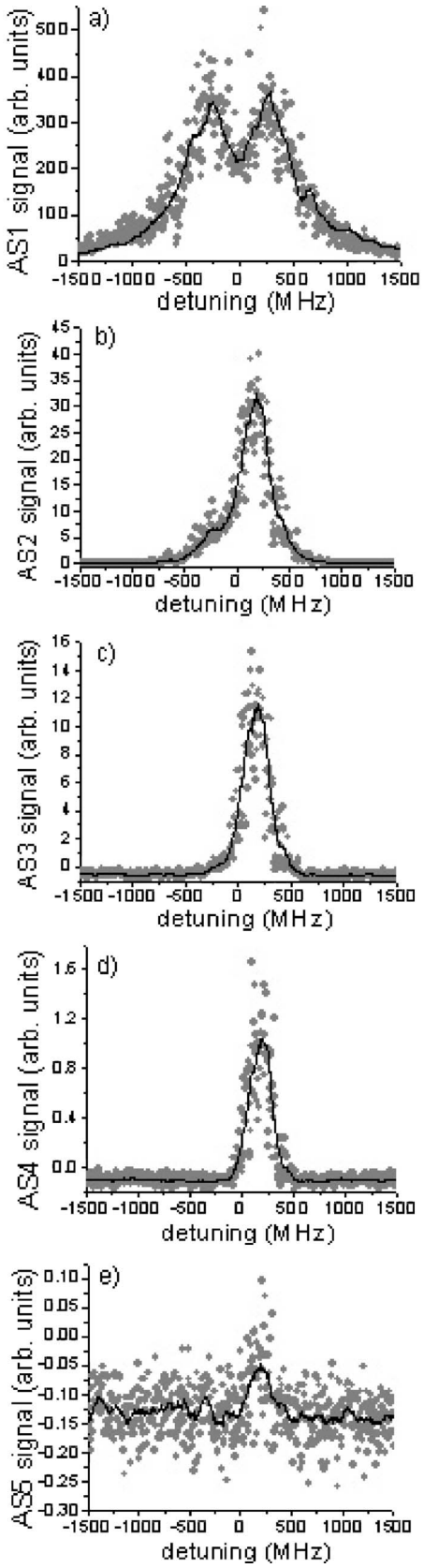

FIG. 6. Dependence of sideband signals on δ_s of driving fields (long focusing geometry); sideband (a) AS1, (b) AS2, (c) AS3, (d) AS4, and (e) AS5. Black line shows 20-point smoothing of data.

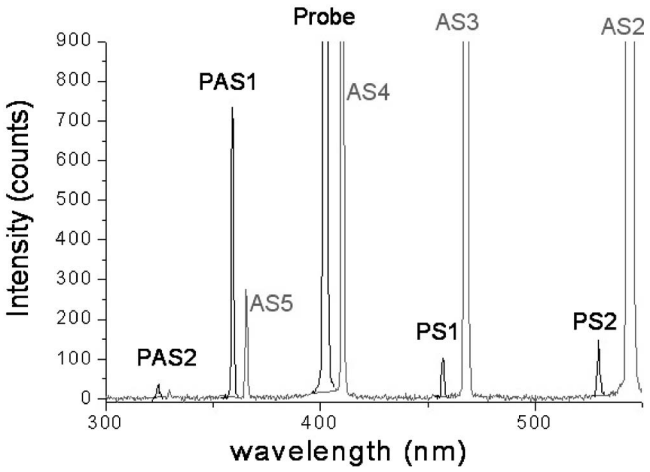

FIG. 7. Raw spectral output resulting from propagation of probe pulse through coherently prepared sample. Features in black are those observable only when probe pulse is present. Features in gray are also present if the probe field is blocked.

single-peaked structure as δ_s is varied, in contrast to the double-peak structure observed for the low-order sidebands of the driving fields. This point is discussed further in Sec. V.

The dependence of the conversion efficiency from the probe field into its highest-order observable sideband (PAS2) on the two-photon Rabi frequency of the driving fields (Ω_{ab}) is shown in Fig. 9. An increase in conversion efficiency is observed as Ω_{ab} increases. This implies that, although nonadiabatic behavior will be driven more strongly for high Ω_{ab}, the overall effectiveness of the modulator is still increasing as the coherence strengthens.

We next use the probe field to investigate the temporal behavior of the system. The dependence of the generated intensity of probe field sidebands PAS1 and PS1 on the delay of this pulse with respect to the driving fields (at a constant value of δ_s) is shown in Fig. 10. This figure clearly shows that both sidebands are generated with highest intensity at a probe field delay of 1.5 ± 0.5 ns, that is, when the probe field is timed to arrive 1.5 ns after the peak of the driving field pulses. This was a somewhat surprising result, but was found to be repeatable. No observable effect on the driving field sidebands was found as the delay was varied, indicating that the coherence prepared by the driving fields was constant throughout.

Le Kien *et al.* [15] have predicted that if there is nonadiabatic behavior in the evolution of the system, the sample-averaged coherence may reach its maximum value some time after the peak of the driving field pulses. In order to investigate this effect further, the pump field energy was decreased such that its intensity was 0.30 GW cm^{-2}, conditions under which the evolution has been shown to be more fully adiabatic (Table I). A delay scan was then carried out, the results of which are shown in Fig. 11. It is clear that the delay producing the maximum probe field sideband signal is decreased to 0.3 ± 0.5 ns when employing the lower pump field energy. The reduced delay necessary to produce strongest modulation of the probe field under these conditions is consistent with the evolution of the system being more adiabatic [15].

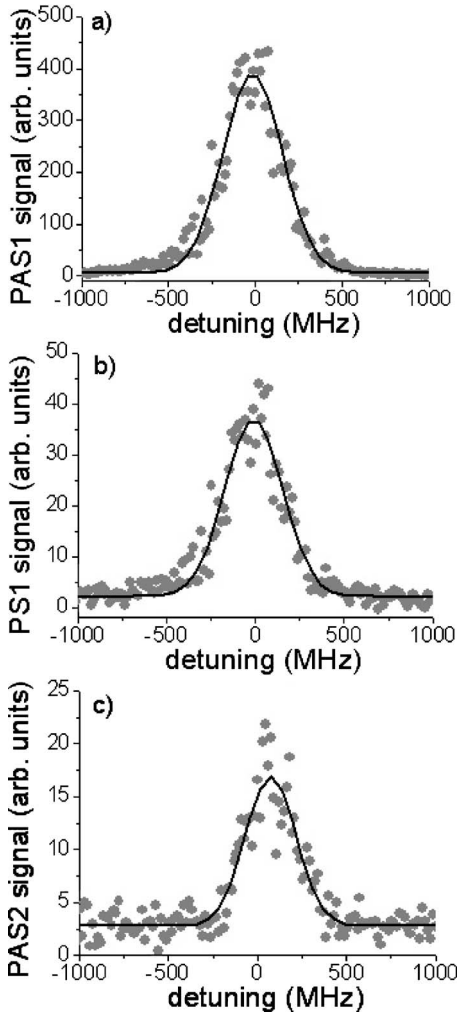

FIG. 8. Dependence of (a) PAS1, (b) PS1, and (c) PAS2 sideband signals on two-photon detuning of driving fields. Black lines show Gaussian fit to data.

Figures 10 and 11 also show that very little probe field sideband generation is observed for delays greater than the pulse duration of the pump field. This implies that the evolution of the system is primarily adiabatic in both cases, and is consistent with the observation that only approximately 3% of the energy in the driving fields is lost through lack of adiabaticity at small two-photon detunings.

C. Modulation of a high-power ultrashort probe pulse

We next present results concerning the modulation of the ultrashort probe pulse in the coherently prepared medium. At pressures of 150–250 mbar, and maximum driving field intensities, we observe the generation of two Stokes and two anti-Stokes sidebands of the ultrashort probe field, while the generation of the driving field sidebands appears to proceed as normal (Fig. 12). If the ultrashort probe field was the only field propagated through the cell, no modulation was observed. Very little effect on the generation of the probe field sidebands was found as the temporal delay of the ultrashort pulse was varied with respect to the driving fields over a range of ±2 ns.

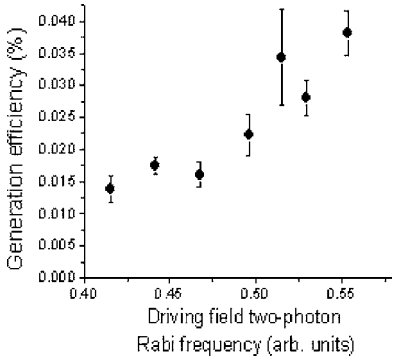

FIG. 9. Efficiency with which energy is transferred from probe field to sideband PAS2 as a function of the two-photon Rabi frequency of the driving fields.

Figure 13 shows how the generated PAS1, PAS2, and PS1 probe field sideband signals depend on the two-photon detuning of the driving fields (δ_s). As for all other fields investigated, the most efficient modulation of the probe field is found to occur at a nonzero value of δ_s: this confirms that the sideband generation is due to the coherent enhancement, rather than a standard four-wave-mixing process. The maximum total conversion efficiency from the probe field into all sidebands observed is $7.5 \pm 0.8\,\%$, occurring at $\delta_s = 19 \pm 13$ MHz. The total conversion efficiency into all sidebands at the detuning which maximizes the generation of the higher-order sidebands ($\delta_s = 190 \pm 38$ MHz) is measured as $6.1 \pm 0.9\,\%$. As for the narrowband probe field, no local minimum centered at $\delta_s = 0$ is observed in the PAS1 and PS1 sideband signals. This point is discussed further in Sec. V.

Figure 14 shows the dependence of the conversion efficiency from the probe field into sideband PAS1 on the two-photon Rabi frequency with which the driving fields prepare the modulator (Ω_{ab}), at a constant value of the detuning. The input probe field intensity was monitored to be constant to within 5 % while this data was recorded. Each point represents an average of ten output spectra. A steady increase in

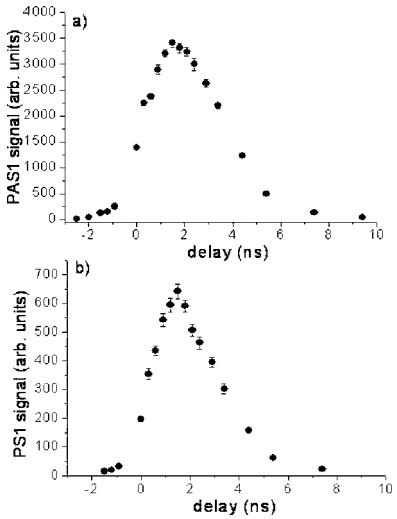

FIG. 10. (a) PAS1 and (b) PS1 signal recorded as delay of probe pulse is varied.

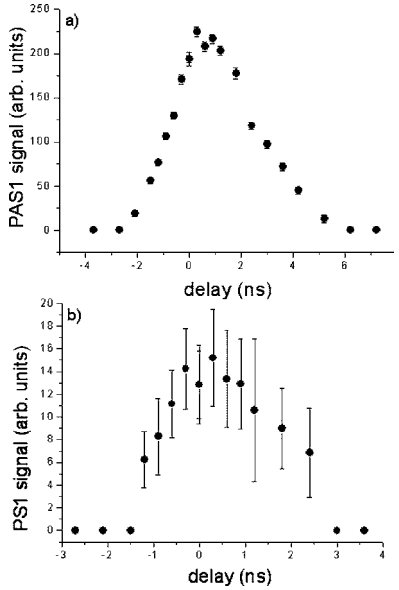

FIG. 11. (a) PAS1 and (b) PS1 signal recorded as delay of probe pulse is varied, for low-intensity driving fields as described in text.

the conversion efficiency into sideband PAS1 is observed as Ω_{ab} increases. This is consistent with modulation of the probe field being enabled by the coherence prepared by the driving fields.

We also observed that the generated intensity of the probe field sidebands was increased if the input probe field intensity was increased. Figure 15 shows the variation in the conversion efficiency from the 130 fs probe field into sidebands PAS1 and PS1 as the input intensity of the probe field is varied. Within error, the gradient of linear fits to both sets of data is zero, and thus the probe field modulation efficiency is found to be independent of its input intensity. This implies that the modulator does not change in any measurable way as the applied probe field intensity is increased.

To gain further insight into the probe field modulation process, the 397 nm field was temporally stretched by propagation through 15 cm of fused silica prior to injection into the cell. A simple calculation based on the optical properties

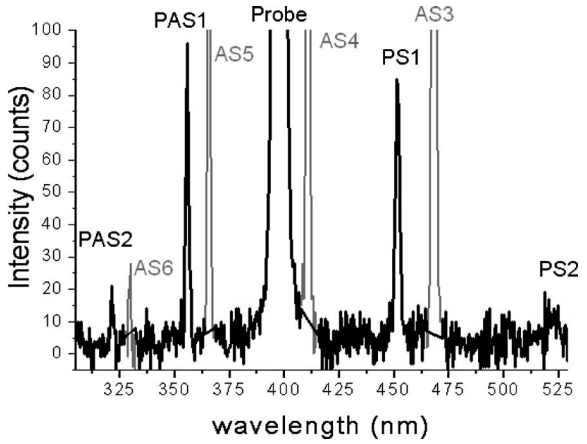

FIG. 12. Output spectrum of combined probe and driving field system for δ=196±37 MHz.

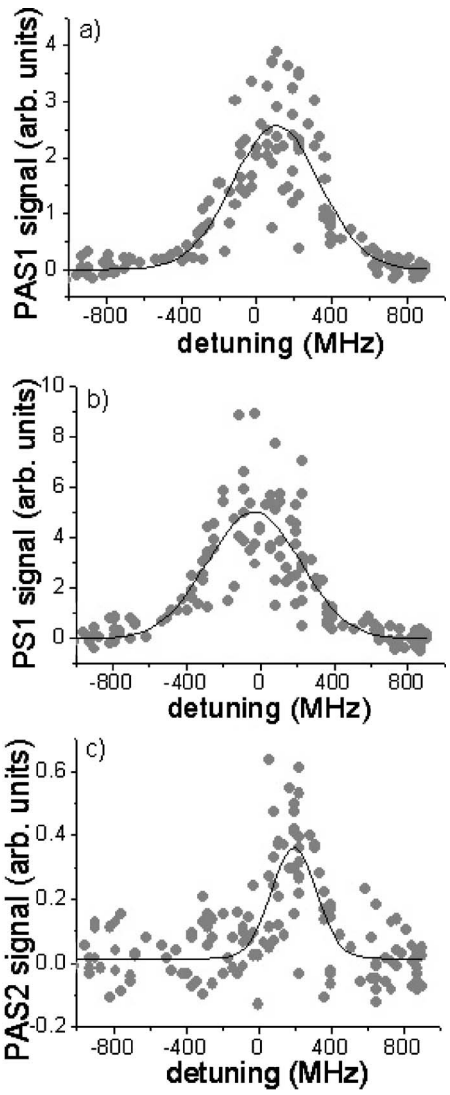

FIG. 13. Probe field sideband signal dependence on two-photon detuning of driving fields. Sideband (a) PAS1, (b) PS1, and (c) PAS2. Each point represents the sum of ten laser shots. Black line shows Gaussian fit to data.

of fused silica gives that the resultant probe field has a pulse duration of 900 fs, and peak intensity of 1.5 GW cm^{-2} (for pulse energy of 250 μJ). The output spectrum of the system was not noticeably affected as a result of stretching the ultrashort probe pulse. Figure 16 shows the detuning characteristics of the probe field sidebands generated. The maximum conversion efficiencies from the probe field into its sidebands were found to be 2.0±0.6 % at δ_s=82±34 MHz, 3.8±0.9 % at δ_s=−71±36 MHz, and 0.8±0.6 % at δ_s =259±37 MHz for sidebands PAS1, PS1, and PAS2, respectively. Both the measured conversion efficiencies and values of δ_s yielding the strongest generation of each sideband agree well with the values found for the original unstretched probe field.

In order to investigate the modulation of the shortest-duration probe pulses available, the doubling crystal used to generate the 400 nm beam was replaced by a thinner (1-mm-thick) KDP crystal, producing probe pulses at

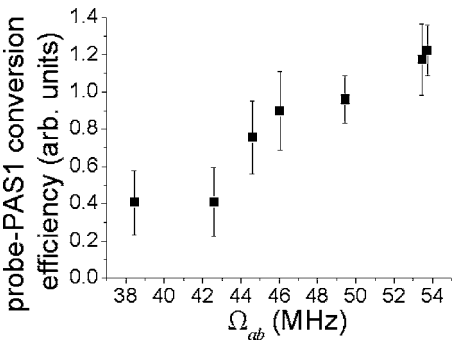

FIG. 14. Dependence of conversion efficiency from probe field into sideband PAS1 on the two-photon Rabi frequency of the driving fields.

397 nm with a pulse duration of roughly 70 fs. The output spectrum observed when propagating this shorter duration probe pulse through the coherently prepared sample is shown in Fig. 17. It is clear that probe field sideband generation is inhibited as compared to the 130 fs probe pulse case; the signal of both sidebands PAS1 and PS1 is reduced by a factor of roughly 2. In addition, sideband PAS1 shows a sharp dip that spectrally splits it into two peaks. It was found that this dip was present in sideband PAS1 under all accessible driving field and probe field parameters, and always occurred at the wavelength corresponding to the center of the sideband. However, the shape of the double-peaked structure, such as depth of the dip and relative heights of the two peaks, varied strongly on a shot-to-shot basis. No such structure was observed in the spectrum of the probe pulse itself.

To test whether this feature in the sideband generation was due to the shorter pulse duration of the probe pulse, the pulse was stretched by propagation through fused silica blocks (4 and 15 cm in length, resulting in stretched pulse durations of roughly 210 fs and 1.1 ps, respectively) before being introduced to the cell. However, a sharp dip at the center of the first anti-Stokes sideband was still observed in every output spectrum recorded, as shown in Fig. 18. It was therefore concluded that this effect was not due to the shorter pulse duration resulting from the use of the thinner doubling crystal, but to the larger bandwidth of the resulting probe field pulses. This issue is discussed further in Sec. V.

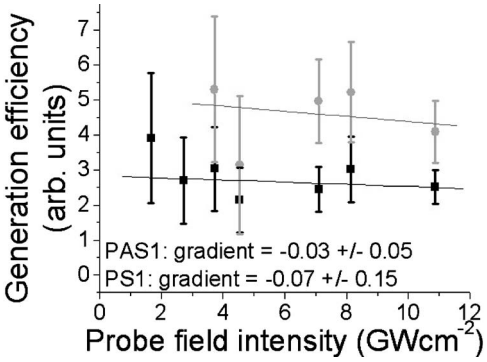

FIG. 15. Conversion efficiency from probe field into its first-order sidebands.

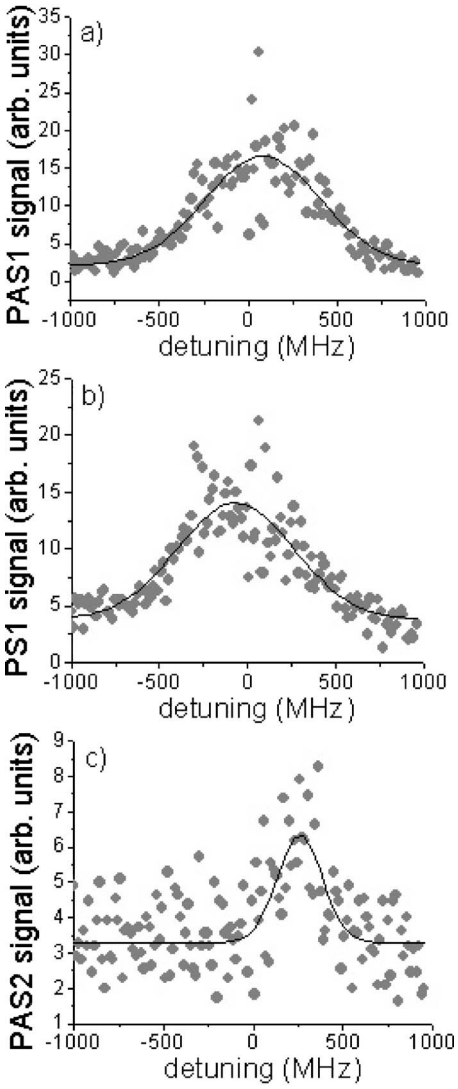

FIG. 16. Detuning characteristics of sidebands of temporally stretched probe pulse. Sideband (a) PAS1, (b) PS2, and (c) PAS2. Black line shows Gaussian fit to data.

V. DISCUSSION

Although the single-molecule coherence predicted by Eq. (9) is maximal if $\delta_s=0$, we observe in all our investigations that Raman sidebands are generated most efficiently at a nonzero value of δ_s. In the case of the driving fields, the loss of modulation efficiency at small detunings was attributed to nonadiabatic behavior in the evolution of the system. This was confirmed experimentally, the nonadiabatic behavior depending on the experimental parameters as predicted by Eq. (13), and is consistent with previous work in this field [10]. Our detailed investigations have allowed greater insight to be gained into the role of nonadiabatic behavior in this system, and in particular have highlighted the delicacy of the balance between adiabatic evolution and the generation of a strong coherence.

We observed that, although the extent of the nonadiabatic following is small (fractional energy <0.03), it is sufficient to decrease the sideband yield to almost zero on resonance.

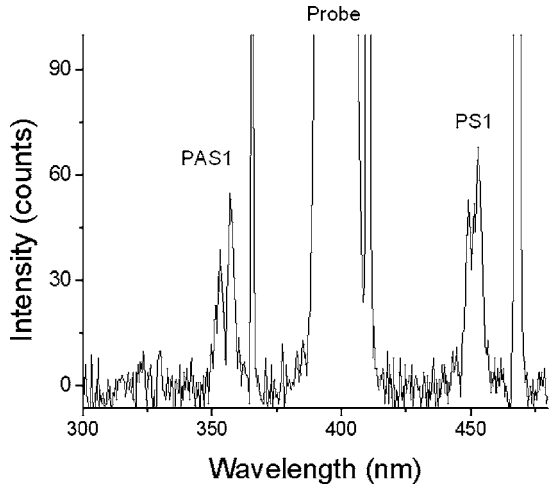

FIG. 17. Output spectrum resulting from propagation of 70 fs probe pulse through the coherently prepared sample.

For the production of a broadband Raman spectrum, it is therefore imperative that the coherence be prepared by driving fields tuned to a nonzero value of δ_s [Eq. (13)]. However, as can be seen from Figs. 3 and 5, a broadband Raman spectrum is not generated if too large a two-photon detuning is employed, since the material coherence weakens as the detuning increases [Eq. (9)]. The importance of achieving both a strong coherence and adiabatic following is therefore clear: the highest-order sidebands observed are generated over a detuning range of only ~350 MHz (full width at half maximum).

For both focusing conditions investigated, the nature of the driving field sideband generation was found to be very similar. High-order anti-Stokes sidebands were generated most efficiently if the medium was prepared in the phased superposition state, contrary to theoretical predictions based on the effect of dispersion [15]. However, the observed behavior is consistent with that found by Harris and co-workers [10,11], indicating that Raman self-focusing may play a role in the generation of the higher-order sidebands. In contrast, the lower-order sidebands are generated most efficiently if the medium is prepared in the antiphased superposition state. This effect has also been observed by Sokolov *et al.* [10], and may be due to reduced depletion of the lower-order sideband energies as the higher-order sidebands cease to be generated.

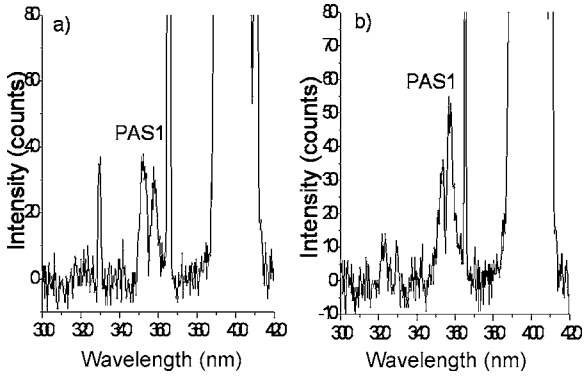

FIG. 18. Output spectrum for 70 fs probe pulse stretched by (a) 15 cm and (b) 4 cm fused silica block.

Small differences were observed in the behavior of the modulator for each focusing case, and these were consistent with the different driving field two-photon Rabi frequencies applied. For instance, although evidence of nonadiabatic behavior was found in both cases, this effect was found to be less severe for the longer-focal-length case, in which the driving fields are applied with a smaller two-photon Rabi frequency [Eq. (13)]. Also, in the tighter focusing case, the sidebands were observed over a larger range of detunings: this is consistent with the coherence depending less strongly on detuning for the setup in which the two-photon Rabi frequency of the driving fields is highest [Eq. (9)]. The highest modulation efficiencies observed, expressed as the ratio of the AS4 to AS1 signals, were 0.33 ± 0.09 % for the loose focusing geometry, and 0.75 ± 0.04 % for the tighter focusing case. The shorter focusing geometry therefore results in sideband production that is roughly twice as efficient at similar pressures. This indicates that, although the optimum detuning in our experiment takes a value that is not large enough for complete adiabatic following of the system, it is beneficial to increase the two-photon Rabi frequency of the driving fields (Ω_{ab}) to increase the strength of the coherence, rather than decrease it to improve the level of adiabatic following. A modulator prepared using the shorter focusing geometry is therefore expected to modulate a probe field more efficiently.

Modulation of a narrowband probe pulse has been successfully demonstrated; sidebands of this field covering a wavelength range 324–526 nm have been generated with an efficiency approaching 1 %. Modulation of a 130 fs probe pulse in the coherently prepared sample has also been successfully observed, resulting in the generation of sidebands spanning a bandwidth of 360 THz, at an efficiency of roughly 6 %. For both probe fields, it was observed that the modulation efficiency depends on the driving field intensities, and that no sidebands of the probe field are generated if the driving fields are not applied. We also observed that the efficiency with which both probe fields were modulated maximized at a nonzero value of δ_s. These three observations provide experimental confirmation that preparation of a material coherence is the key mechanism in the frequency modulation process. It was also observed that the efficiency with which sidebands of the ultrashort field were generated was independent of the probe field intensity. This indicates that the coherence generated by the driving fields was robust to the presence of the high-intensity ultrashort probe field, implying that the probe field intensity could be further increased without causing significant disturbance of the coherence.

We have observed that the detuning characteristics of all probe field sidebands exhibit a single-peaked structure. This is in contrast to the behavior of the low-order driving field sidebands, for which a double-peaked structure was observed as detuning was varied: this feature was attributed to nonadiabatic behavior at small detunings. If the probe fields are affected by nonadiabatic behavior in the same way as the driving fields (as indicated by the similar value of detuning required to produce optimum modulation of all fields), one might expect a similar feature to be present. However, the

sideband signals of the probe fields are roughly an order of magnitude lower than that of the driving fields, and the shot-to-shot variation is greater. Evidence of nonadiabatic behavior is thus harder to detect, and may be revealed if probe fields of greater intensity are employed.

Although the modulation of the two probe fields exhibited similar qualitative behavior, significant differences were also observed. First, higher conversion efficiencies were achieved in the case of the ultrashort field. Second, while the optimum value of the driving field two-photon detuning for efficient modulation of the ultrashort probe field (196 ± 37 MHz) was found to correspond well to that producing the most effective modulation of the driving fields themselves (204 ± 30 MHz), modulation of the narrowband probe field was found to be most efficient if the medium was prepared significantly closer to two-photon resonance ($\delta_s = 74.6 \pm 30.0$ MHz). These results indicate that the material coherence threshold for modulation of the narrowband probe field is higher than for modulation of the ultrashort probe field. This may be an artifact of the averaging of the coherence over the 3.5 ns probe field pulse duration, which will be lower than peak value of the coherence that is sampled by the 130 fs probe pulse.

Increasing the bandwidth of the ultrashort probe field was found to inhibit the sideband generation process: a sharp dip was consistently observed at the center of the first anti-Stokes probe field sideband. The very deep and narrow nature of the dip may imply that it is caused by a quantum or optical interference effect. Since the bandwidth of the 70 fs probe pulse is large enough to strongly couple rotational states in deuterium through Raman processes, we tentatively suggest that the observed effect could be a result of the creation of an effective three- (or more) level system. It is well known that in such a system, quantum interference effects can lead to the complete cancellation of a dipole moment on resonance [7]. However, although the shape of the first Stokes sideband becomes rather irregular, the strong splitting is not observed in this sideband. The origin of this feature remains to be explained: this may require a more complete modeling of the propagation of the laser fields taking into account rotational as well as vibrational states.

The modulation of the narrowband probe pulse has allowed greater insight into the temporal behavior of the modulator to be gained. We find that frequency modulation of the probe pulse is not necessarily most efficient at the point in the evolution of the modulator when the two-photon Rabi frequency of the driving fields is largest. Rather, modulation was found to be most efficient at later times. This may be attributed to the small degree of nonadiabaticity in the system. Further experimental investigation is necessary to provide a complete picture of this mechanism.

VI. CONCLUSIONS

We have conducted detailed experimental investigations into off-resonant preparation of a vibrational coherence, by analysis of the high-order stimulated Raman scattering occurring in the system. We have determined that, even employing driving fields of relatively low two-photon Rabi frequency, there is nonadiabatic behavior in the evolution of the system at small-magnitude two-photon detunings. This has a significant effect on the number of Raman sidebands generated in the sample: we observe only weak generation of low-order anti-Stokes sidebands if the coherence is prepared with driving fields tuned $< \sim 150$ MHz from two-photon resonance, even though the prepared coherence is strongest in this region. If the detuning is too large, the coherence becomes weak, and again a strongly modulated spectrum is not generated. For our experimental parameters, we find that an acceptable compromise between these two conflicting requirements is attained over a range of detunings of only 350 MHz. We have also used an independent probe field to interrogate the coherence prepared, and discovered that the temporal evolution of the coherence may be strongly affected by nonadiabatic behavior in the system.

We have observed efficient modulation of both a narrowband probe field, and an ultrashort probe field, in the coherently prepared medium, resulting in the generation of Raman sidebands covering 360 THz of bandwidth in both cases. It is apparent that for both probe fields a real benefit would have been gained in terms of the modulation efficiencies achieved had it been possible to further increase the two-photon Rabi frequency of the driving fields beyond the value accessed in this work. This would have allowed an even greater bandwidth to be generated. Increasing the probe field energy injected into the cell would also be a valuable improvement that would potentially increase the bandwidth covered by the probe field sidebands. In our experiment, the energies of all fields injected into the cell was limited only by the damage threshold of the cell windows: a problem that should be relatively easy to overcome.

The modulation of probe fields in the coherently prepared sample has possible application in the generation of tunable subfemtosecond pulse trains, and also in the efficient generation of tunable radiation in the uv. In particular, although a temporal diagnosis of the output has not been carried out in this work, we have calculated that if the phases of the sidebands resulting from the modulation of the ultrashort probe pulse at the exit of the cell were adjusted such that they share a common value, a train of roughly 11 pulses, each of duration 2.8 fs, and easily focusable to an intensity of 2.5×10^{13} W cm^{-2} may be synthesized [17]. This scheme therefore represents a potentially useful source of high-power, few-cycle pulses. With improvement, high-power, isolated subfemtosecond pulses may be produced from this system. The insights into the coherence preparation process presented here are an essential step if this goal is to be realized.

We gratefully acknowledge the contributions of J. Roos, and the technical support of P. Ruthven and A. Gregory. This work was funded by UK EPSRC.

[1] M. Fleischauer, A. Imamoglu, and J. P. Marangos, Rev. Mod. Phys. **77**, 633 (2005).
[2] Andrew Merriam *et al.*, Phys. Rev. Lett. **84**, 5308 (2000).
[3] T. Rickes *et al.*, J. Chem. Phys. **113**, 534 (2000).
[4] K. Bergmann, H. Theuer, and B. W. Shore, Rev. Mod. Phys. **70**, 1003 (1998).
[5] G. Z. Zhang, D. W. Tokaryk, B. P. Stoicheff, and K. Hakuta, Phys. Rev. A **56**, 813 (1997).
[6] Maneesh Jain *et al.*, Phys. Rev. Lett. **77**, 4326 (1996).
[7] A. Kasapi, Maneesh Jain, G. Y. Yin, and S. E. Harris, Phys. Rev. Lett. **74**, 2447 (1995).
[8] S. E. Harris, Opt. Lett. **19**, 2018 (1994).
[9] S. E. Harris and A. V. Sokolov, Phys. Rev. A **55**, R4019 (1997).
[10] A. V. Sokolov *et al.*, Phys. Rev. Lett. **85**, 562 (2000).
[11] D. D. Yavuz, D. R. Walker, G. Y. Yin, and S. E. Harris, Opt. Lett. **27**, 769 (2002).
[12] J. Q. Liang, M. Katsuragawa, Fam Le Kien, and K. Hakuta, Phys. Rev. Lett. **85**, 2474 (2000).
[13] S. E. Harris and A. V. Sokolov, Phys. Rev. Lett. **81**, 2894 (1998).
[14] M. Y. Shverdin *et al.*, Phys. Rev. Lett. **94**, 033904 (2005).
[15] Fam Le Kien *et al.*, Phys. Rev. A **60**, 1562 (1999).
[16] Fam Le Kien, Nguyen Hong Shon, and K. Hakuta, Phys. Rev. A **64**, 051803(R) (2001).
[17] Sarah Gundry *et al.*, Opt. Lett. **30**, 180 (2005).
[18] Fam Le Kien, K. Hakuta, and A. V. Sokolov, Phys. Rev. A **66**, 023813 (2002).
[19] A. V. Sokolov *et al.*, Phys. Rev. A **63**, 051801(R) (2001).
[20] Emiliano Sali *et al.*, Opt. Lett. **29**, 495 (2004).
[21] A. Nazarkin, G. Korn, M. Wittmann, and T. Elsaesser, Phys. Rev. Lett. **83**, 2560 (1999).
[22] N. Zhavoronkov and G. Korn, Phys. Rev. Lett. **88**, 203901 (2002).
[23] D. R. Walker *et al.*, Opt. Lett. **27**, 2094 (2002).
[24] W. R. Bosenberg and Dean R. Guyer, J. Opt. Soc. Am. B **10**, 1716 (1993).
[25] K. Hakuta, M. Suzuki, M. Katsuragawa, and J. Z. Li, Phys. Rev. Lett. **79**, 209 (1997).